Some of the electron density may have been transferred to the Na^+ cation.

Concluding remarks

The influence of sodium cations on coordinated lone-pair deformation densities is too strong to be neglected. In the case of UH-AF 50 NA the sodium cation seems to weaken the densities of most of the lone pairs. The influence of hydrogen bonds may be much lower. Therefore it would be interesting to measure the deformation density of the ammonium or amine salts of the title compound.

This work has been funded by the German Federal Minister for Research and Technology (BMFT) under contract No. 03-LU1 FUB-0-F1-55 and by the Fonds der Chemischen Industrie. We thank Dr Hans-Ullrich Wagner, Institute of Organic Chemistry, University of Munich, for helpful advice.

References

FRISCH, M. J., BINKLEY, J. S., SCHLEGEL, H. B., RAGHAVACHARI, K., MELIUS, C. F., MARTIN, R. L., STEWART, J. J., BOBROWICZ, F. W., ROHLFING, C. M., KAHN, L. R., DEFREES, D. J., SEEGER, R., WHITESIDE, R. A., FOX, D. J., FLUDER, E. M. & POPLE, J. A. (1984). *GAUSSIAN86*. Carnegie-Mellon Quantum Chemistry Publishing Unit, Pittsburgh, PA, USA.

KELLER, E. (1988). *SCHAKAL88. A FORTRAN Program for the Graphic Representation of Molecular and Crystallographic Models*. Univ. of Freiburg, Germany.

OLOVSSON, I. (1982). *Croat. Chem. Acta*, **55**, 171–190.

RUDERT, R., BUSCHMANN, J., LUGER, P., GREGSON, D. & TRUMMLITZ, G. (1988). *Acta Cryst.* C**44**, 1083–1086.

RUDERT, R., BUSCHMANN, J., LUGER, P., GREGSON, D. & TRUMMLITZ, G. (1989). *Acta Cryst.* C**45**, 1013–1015.

SCHOMAKER, V. & TRUEBLOOD, K. N. (1968). *Acta Cryst.* B**24**, 63–76.

STEWART, J. M. & HALL, S. R. (1986). Editors. *The XTAL System of Crystallographic Programs*. Tech. Rep. TR-1364.2. Computer Science Center, Univ. of Maryland, College Park, Maryland, USA.

STEWART, R. F., DAVIDSON, E. R. & SIMPSON, W. T. (1965). *J. Chem. Phys.* **42**, 3175–3187.

WANG, Y. & LIAO, J. H. (1988). *Acta Cryst.* B**45**, 65–69.

ZACHARIASEN, W. H. (1967). *Acta Cryst.* **23**, 558–564.

Acta Cryst. (1991). B**47**, 910–917

Electron-Density Distribution in *lel*$_3$- and *ob*$_3$-Tris(*trans*-1,2-diaminocyclohexane)-cobalt(III) Nitrate Trihydrate at 120 K

BY MITSUO MOROOKA, SHIGERU OHBA* AND YOSHIHIKO SAITO

Department of Chemistry, Faculty of Science and Technology, Keio University, Hiyoshi 3-14-1, *Kohoku-ku, Yokohama* 223, *Japan*

AND HIROSHI MIYAMAE

Department of Chemistry, Faculty of Science, Josai University, Keyakidai 1-1, *Sakado-shi, Saitama* 350-02, *Japan*

(*Received* 19 *February* 1991; *accepted* 11 *June* 1991)

Abstract

The electron-density distribution in two optically active Co^{III} complexes with *trans*-1,2-diaminocyclohexane (chxn) as a bidentate ligand have been investigated by the multipole-expansion method based on X-ray intensities collected at 120 K with Mo $K\alpha$ radiation ($\lambda = 0.71073$ Å). Crystals of the *lel*$_3$- and *ob*$_3$-conformers are isotypic and hexagonal $P6_3$, $Z = 2$, $R = 0.038$ and 0.033 for 3916 and 1831 reflections, respectively. $[Co(R,R\text{-chxn})_3](NO_3)_3.3H_2O$, $M_r = 641.6$, $F(000) = 684$. (I): $\Delta(\lambda\lambda\lambda)$-complex (*lel*$_3$-isomer), $a = 12.998$ (3), $c = 9.973$ (3) Å, $V = 1459.2$ (8) Å^3, $D_x = 1.46$ Mg m^{-3}, $\mu = 0.653$ mm^{-1}. (II): $\Lambda(\lambda\lambda\lambda)$-complex (*ob*$_3$-isomer), $a = 13.192$ (1), $c = 9.787$ (2) Å, $V = 1475.0$ (5) Å^3, $D_x = 1.44$ Mg m^{-3}, $\mu = 0.646$ mm^{-1}. The aspherical 3*d*-electron distribution around the Co atom is essentially the same as that of the octahedral complex for both isomers and significant chirality was not observed. The necessity of phase improvement for the deformation density around the Co atom in the non-centrosymmetric structures depends on the symmetry of the multipole densities. The features of the multipole density, hexadecapole y_{40}, are not smeared by the use of the independent atom model (IAM) phase because the phase of the y_{40} contribution to the structure factor coincides with that of the cobalt monopole. On the other hand, the features of y_{43} are much affected by the phase error. Incompleteness of the Fourier series within the $(\sin\theta/\lambda)_{max}$ in the

* To whom correspondence should be addressed.

0108-7681/91/060910-08$03.00

calculation of the deformation density produces an artificial imbalance of the peak heights of the aspherical *d*-electron distribution.

Introduction

As an extension of our systematic studies on the aspherical *d*-electron distribution in transition-metal complexes (Takazawa, Ohba & Saito, 1988; and references therein), we have investigated trisbidentate Co^{III} complexes. The title crystals are suitable for this purpose because the metal complexes have crystallographic threefold symmetry and the puckering motion of the chelate rings is prevented by the rigid chair form of the cyclohexane moiety in the ligand. Racemic crystals could not be obtained because of spontaneous resolution. Since the crystal structure is non-centrosymmetric, phase improvement was achieved by the multipole-expansion method (Hansen & Coppens, 1978).

A preliminary study on the crystal structure and the electron-density distribution of $[Co(chxn)_3]^{3+}$ (Miyamae, 1977) and $[Rh(chxn)_3]^{3+}$ complexes (Miyamae, Sato & Saito, 1977) was carried out at room temperature. In the present study, crystals of the Co^{III} complexes were cooled to 120 K in order to reduce the thermal smearing.

Experimental

Data collection

Crystals of $\Delta(\lambda\lambda\lambda)$- and $\Lambda(\lambda\lambda\lambda)$-$[Co(R,R\text{-}chxn)_3](NO_3)_3.3H_2O$ were kindly supplied by Dr F. Galsbøl of H. C. Ørsted Institute, University of Copenhagen. They are orange–red hexagonal prisms.

(I): A crystal shaped into a sphere of 0·62 mm in diameter was kept at 120 K with cold nitrogen gas. X-ray intensities were measured on a Rigaku AFC-5 four-circle diffractometer with graphite-monochromatized Mo $K\alpha$ radiation, θ–2θ scan technique with scan speed 6° min^{-1} in θ and scan width $(1{\cdot}3 + 0{\cdot}36\tan\theta)°$. Range of indices, $-18 \le h$, $k \le 18$, $0 \le l \le 14$ $(4 < 2\theta \le 60°)$; $0 \le h$, $k \le 28$, $0 \le l \le 21$ $(60 < 2\theta \le 100°)$. Variation of standard reflections, $0{\cdot}993 < |F_o|/|F_{o\,\text{initial}}| < 1{\cdot}006$, 12 978 reflections measured: 10 943 reflections observed with $|F_o| > 3\sigma(|F_o|)$; 3916 unique reflections ($R_{int} = 0{\cdot}016$ for 1555 reflections). Lattice constants were determined based on 25 2θ values $(23 < 2\theta < 30°)$. Analytical corrections for absorption were made with $\mu r = 0{\cdot}203$ assuming a spherical crystal shape (relative transmission factors $0{\cdot}74 < A < 0{\cdot}75$).

(II): Intensity data were collected at 120 K from an as-grown crystal of approximate dimensions 0·3 × 0·4 × 0·4 mm. Range of indices, $-18 \le h$, $k \le 18$, $0 \le l \le 13$ $(4 < 2\theta \le 60°)$; $0 \le h$, $k \le 21$, $0 \le l \le 15$ $(60 < 2\theta \le 70°)$. $0{\cdot}994 < |F_o|/|F_o|_{\text{initial}} < 1{\cdot}009$, 9898 reflections measured: 8297 reflections observed with $|F_o| > 3\sigma(|F_o|)$; 1831 unique reflections ($R_{int} = 0{\cdot}030$ for 1385 reflections) after analytical absorption corrections $(0{\cdot}84 < A < 0{\cdot}87)$ by the Gaussian numerical integration method (Busing & Levy, 1957).

Table 1. *Refinement information for (A) the conventional refinement with RADIEL and (B) the multipole refinement with MOLLY*

	(I) lel_3-isomer		(II) ob_3-isomer	
	A	*B*	*A*	*B*
No. of reflections	3916	3916	1831	1831
No. of parameters	184	319	184	319
$R(F)$	0·043	0·038	0·041	0·033
$wR(F)$	0·036	0·027	0·037	0·026
S	1·26	0·98	1·40	1·08

Conventional refinement

Conventional refinement was performed with the full-matrix least-squares program *RADIEL* (Coppens, Guru Row, Leung, Stevens, Becker & Yang, 1979). The function $\sum w(|F_o| - |F_c|)^2$ was minimized with weights $w^{-1} = \sigma^2(|F_o|) +$

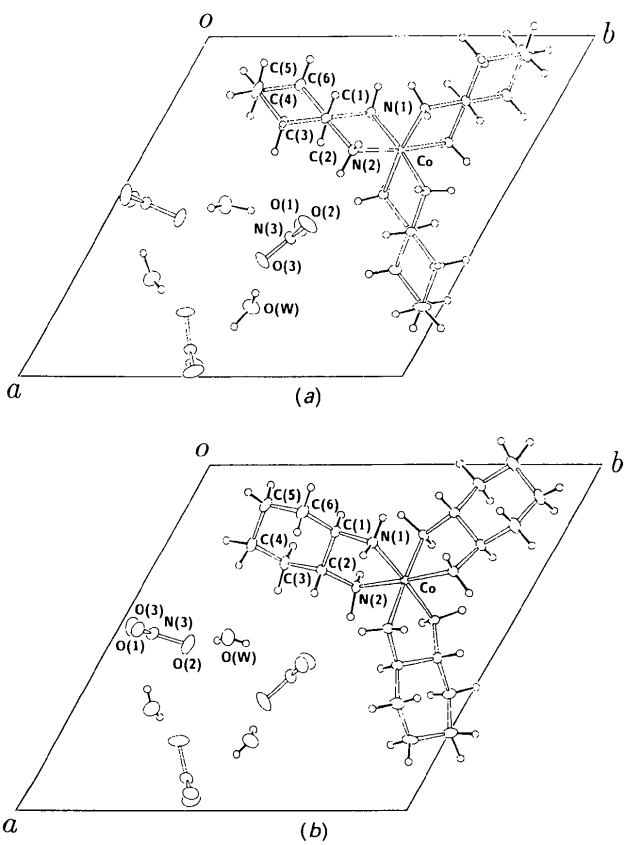

Fig. 1. Partial projection of the crystal structures along the *c* axis. (*a*) $\Delta(\lambda\lambda\lambda)$-complex ($lel_3$-isomer) and (*b*) $\Lambda(\lambda\lambda\lambda)$-complex ($ob_3$-isomer).

Table 2. *Positional parameters* ($\times 10^4$) *and equivalent isotropic temperature factors* (*Hamilton*, 1959)

	x	y	z	B_{eq}(Å^2 × 10)
Compound (I)				
Co	3333	6667	0	6
N(1)	2212 (1)	5331 (1)	−1153 (1)	9
N(2)	3333 (1)	5439 (1)	1153 (1)	9
C(1)	2361 (1)	4297 (1)	822 (1)	10
C(2)	2376 (1)	4254 (1)	696 (1)	10
C(3)	2523 (1)	3232 (1)	1209 (2)	17
C(4)	1553 (2)	2056 (1)	621 (2)	24
C(5)	1568 (2)	2103 (1)	919 (2)	22
C(6)	1406 (1)	3129 (1)	1411 (1)	15
N(3)	5910 (1)	5097 (1)	990 (1)	13
O(1)	5513 (1)	5358 (1)	1986 (1)	24
O(2)	5600 (1)	5220 (1)	−172 (1)	18
O(3)	6588 (1)	4681 (1)	1136 (1)	18
O(*W*)	7935 (1)	5053 (1)	−1323 (2)	19
Compound (II)				
Co	3333	6667	0	6
N(1)	2220 (2)	5297 (2)	1111 (2)	9
N(2)	3510 (2)	5526 (2)	1115 (2)	9
C(1)	1904 (2)	4213 (2)	312 (3)	12
C(2)	3034 (2)	4410 (2)	352 (3)	12
C(3)	2820 (3)	3371 (3)	−1245 (3)	17
C(4)	2254 (3)	2242 (3)	−410 (4)	22
C(5)	1126 (3)	2045 (3)	266 (4)	25
C(6)	1335 (2)	3091 (3)	1151 (3)	18
N(3)	4849 (1)	949 (1)	−1019 (2)	15
O(1)	4733 (1)	511 (2)	162 (4)	17
O(2)	5176 (2)	2021 (4)	−1147 (2)	22
O(3)	4658 (2)	332 (3)	−2075 (4)	23
O(*W*)	4963 (2)	2945 (2)	1439 (5)	19

$(0{\cdot}015\,F_o|)^2$. The initial atomic coordinates were those of Miyamae (1977). All the H atoms appeared clearly on a difference synthesis. Positional and thermal parameters of non-H atoms were refined using high-order data [(I): $\sin\theta/\lambda > 0{\cdot}7$ Å^{-1} (2507 reflections), (II): $\sin\theta/\lambda > 0{\cdot}55$ Å^{-1} (1113 reflections)]. When an isotropic extinction parameter was introduced (Becker & Coppens, 1974), the g value became $0{\cdot}09\,(3) \times 10^4$ for the lel_3-isomer, and gave a negative value for the ob_3-isomer. Subsequent refinements were carried out without an extinction correction. Complex neutral-atom scattering factors were taken from *International Tables for X-ray Crystallography* (1974, Vol. IV). Refinement information is shown in Table 1. Partial projections of the crystal structures are presented in Fig. 1.

Multipole expansion

Multipoles were included up to the hexadecapole level for Co, O, N and C atoms. The radial functions were $r^n\exp(-\zeta r)$ with $n_l = 4$ for all the l values (Co) and $n_l = 2, 2, 2, 3, 4$ for $l = 0, 1, 2, 3, 4$ (O, N, and C). Core scattering factors were taken from *International Tables for X-ray Crystallography* (1974, Vol. IV). The positional, thermal, multipole and ζ (shielding) parameters were refined with the program *MOLLY* (Hansen & Coppens, 1978). Initial ζ values were taken from Clementi & Raimondi (1963). The 4*s* and 4*p* orbital populations for the Co atom were not taken into account. Chemical symmetry 32 (D_3) was assumed for the complex cation since no apparent chirality was observed in the electron distribution around Co. Symmetry constraints in the multipole parameters were imposed upon NO_3^- (D_{3h}) and H_2O (C_{2v}). The total charge of the unit cell was constrained to be neutral. For H atoms, no multipoles were introduced. The valence-electron populations of the H atoms were fixed at 1·0 in order to avoid unrealistic results. Atomic coordinates are listed in Table 2, bond lengths and angles in Table 3.*

Table 3. *Bond lengths* (Å) *and bond angles* (°)

	(I)	(II)
Co—N(1)	1·983 (1)	1·988 (2)
Co—N(2)	1·967 (1)	1·965 (3)
N(1)—C(1)	1·488 (2)	1·495 (4)
N(2)—C(2)	1·487 (1)	1·482 (3)
C(1)—C(2)	1·515 (1)	1·525 (4)
C(1)—C(6)	1·519 (1)	1·522 (4)
C(2)—C(3)	1·522 (2)	1·528 (5)
C(3)—C(4)	1·531 (2)	1·527 (5)
C(4)—C(5)	1·537 (3)	1·527 (6)
C(5)—C(6)	1·531 (3)	1·533 (5)
N(3)—O(1)	1·242 (2)	1·267 (4)
N(3)—O(2)	1·263 (2)	1·262 (5)
N(3)—O(3)	1·252 (2)	1·261 (4)
N(1)—Co—N(2)	85·8 (1)	85·6 (1)
Co—N(1)—C(1)	107·0 (1)	108·0 (2)
Co—N(2)—C(2)	108·8 (1)	109·1 (2)
N(1)—C(1)—C(2)	105·4 (1)	106·2 (2)
N(1)—C(1)—C(6)	114·0 (1)	114·5 (2)
C(2)—C(1)—C(6)	111·6 (1)	111·1 (3)
N(2)—C(2)—C(1)	106·7 (1)	106·1 (2)
N(2)—C(2)—C(3)	113·3 (1)	113·5 (3)
C(1)—C(2)—C(3)	112·2 (1)	111·4 (2)
C(2)—C(3)—C(4)	110·0 (1)	110·5 (3)
C(3)—C(4)—C(5)	110·8 (1)	110·9 (4)
C(4)—C(5)—C(6)	110·5 (2)	111·7 (3)
C(1)—C(6)—C(5)	110·3 (1)	110·5 (3)
O(1)—N(3)—O(2)	119·8 (1)	119·8 (3)
O(1)—N(3)—O(3)	120·2 (1)	120·9 (3)
O(2)—N(3)—O(3)	120·0 (1)	119·2 (3)

Electron populations of the cobalt 3*d* orbitals are listed in Table 4. They were derived from the multipole coefficients based on the following equations (Holladay, Leung & Coppens, 1983):

$$\begin{aligned} P(a_1) &= 0{\cdot}2P_{00} + 1{\cdot}0392P_{20} + 1{\cdot}3957P_{40} \\ P(e) &= 0{\cdot}4P_{00} - 1{\cdot}0392P_{20} - 0{\cdot}3102P_{40} \\ &\quad \pm 1{\cdot}9746P_{43} \\ P(e') &= 0{\cdot}4P_{00} - 1{\cdot}0856P_{40} \mp 1{\cdot}9746P_{43} \\ P(e_+e'_+ + e_-e'_-) &= -2{\cdot}9394P_{20} + 2{\cdot}1932P_{40} \\ &\quad \mp 1{\cdot}3963P_{43}. \end{aligned} \tag{1}$$

* Lists of structure factors, anisotropic thermal parameters, positional parameters of H atoms, bond lengths and bond angles involving H atoms and multipole parameters have been deposited with the British Library Document Supply Centre as Supplementary Publication No. SUP 54335 (58 pp.). Copies may be obtained through The Technical Editor, International Union of Crystallography, 5 Abbey Square, Chester CH1 2HU, England.

Table 4. *Electron populations for the cobalt d orbitals*

	(I) lel_3-isomer	(II) ob_3-isomer
Total	5·98 (8)	6·7 (1)
a_1	1·71 (6)	1·8 (1)
e	3·12 (12)	3·2 (2)
e'	1·15 (12)	1·7 (2)
$e\,.\,e'.\,+\,e\;e'$	0·23 (14)	0·5 (3)

where the P's with parentheses indicate orbital populations and the P_{lm}'s the multipole parameters. Upper and lower signs correspond to (I) and (II), respectively. Here, the threefold axis is taken as the z axis and the chemical twofold axis, passing through Co and the midpoint between the N(1) and N(2) atoms, is chosen as the x axis in order to constrain the Co multipole densities to D_3 symmetry. Since the local axes were rotated along z by 30° (I) clockwise or (II) counterclockwise from those of Holladay, Leung & Coppens (1983), P_{43+} in their Table 4(*b*) was replaced by (I) $-P_{43-}$ or (II) $+P_{43-}$.

Discussion

Phase improvement

Deformation maps around the Co atom after multipole refinement are shown in Fig. 2. The difference densities after conventional refinement based on the independent atom model (IAM), $\Delta\rho'(\mathbf{r})$, are also presented in Fig. 3. The negative density on the Co—N bond axis became clear after the phase improvement. The charge asphericity around the Co

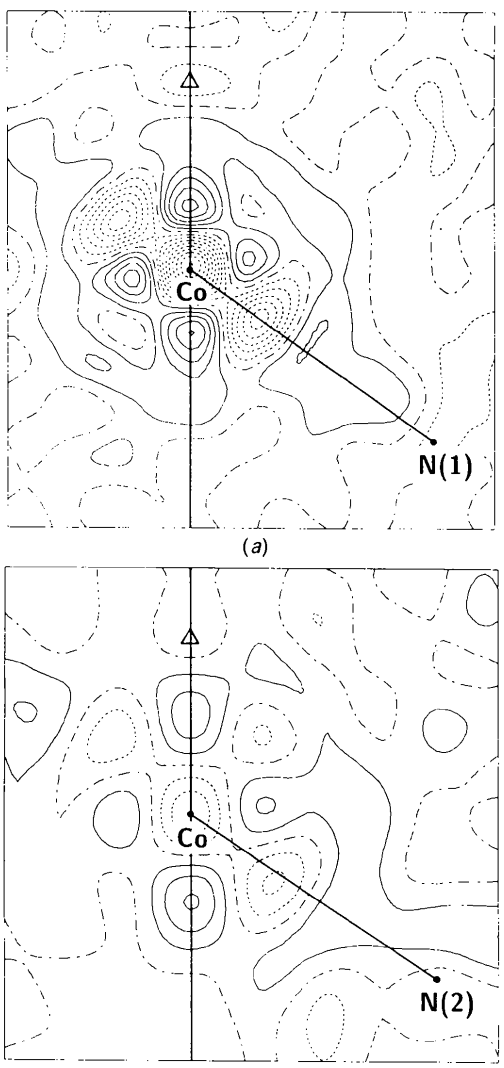

Fig. 2. Observed deformation density after the phase improvement. This is a section through a Co—N bond and the threefold axis. Contour intervals at 0·2 e Å^{-3}. (*a*) lel_3- and (*b*) ob_3-isomer.

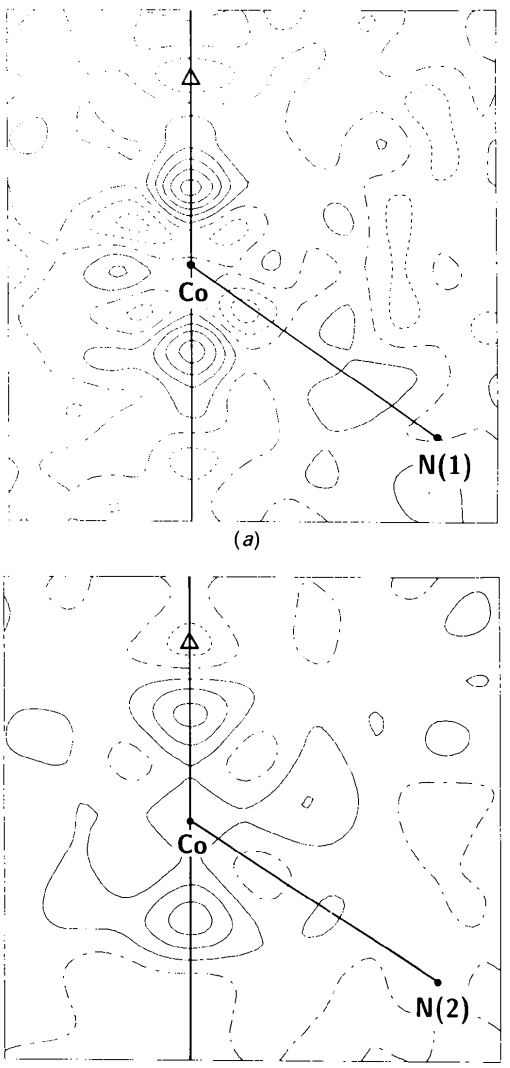

Fig. 3. Difference Fourier synthesis after conventional refinement (without the phase improvement). Contour intervals at 0·2 e Å^{-3}. (*a*) lel_3- and (*b*) ob_3-isomer.

atom is represented mainly with two hexadecapoles, y_{40} and y_{43} (see Figs. 6*a* and 6*b*). The difference density before the phase improvement, $\Delta\rho'(\mathbf{r})$, can be separated approximately into each component of the multipole densities.

$$\begin{aligned}\Delta\rho'(\mathbf{r}) &= \int[|F_{\mathrm{IAM}}(\mathbf{k}) + \sum_{lm}F_{lm}(\mathbf{k})| - |F_{\mathrm{IAM}}(\mathbf{k})|] \\ &\quad \times \exp[i\varphi_{\mathrm{IAM}}(\mathbf{k})]\exp(-2\pi i\mathbf{k}.\mathbf{r})d\mathbf{k} \\ &\simeq \sum_{lm}\int[|F_{\mathrm{IAM}}(\mathbf{k}) + F_{lm}(\mathbf{k})| - |F_{\mathrm{IAM}}(\mathbf{k})|] \\ &\quad \times \exp[i\varphi_{\mathrm{IAM}}(\mathbf{k})]\exp(-2\pi i\mathbf{k}.\mathbf{r})d\mathbf{k} \\ &= \sum_{lm}\rho'_{lm}(\mathbf{r}) \qquad (2)\end{aligned}$$

where $F_{\mathrm{IAM}}(\mathbf{k})$ is the structure factor for the scattering vector $\mathbf{k}$ based on the IAM, $F_{lm}(\mathbf{k})$ the contribution of the multipole density ρ_{lm} in the structure factor. A diagram in Fig. 10 explains the approximation involved in equation (2). The artificial structure factors, $|F_{\mathrm{IAM}}(\mathbf{k}) + F_{lm}(\mathbf{k})|$, were calculated with the refined multipole parameters, P_{40} or P_{43-}, and the independent atom model [$P_{40} = 0{\cdot}13$ (1) and $P_{43-} = 0{\cdot}15$ (2)]. Phase-error free multipole densities $\rho_{40}(\mathbf{r})$ and ρ_{43} (**r**), and the biased densities $\rho'_{40}(\mathbf{r})$ and ρ'_{43} (**r**) are compared in Fig. 6 for the lel_3-conformer. The damping factor c_{lm} can be defined as

$$\rho'_{lm}(\mathbf{r}) \simeq c_{lm}\rho_{lm}(\mathbf{r}) \qquad (3)$$

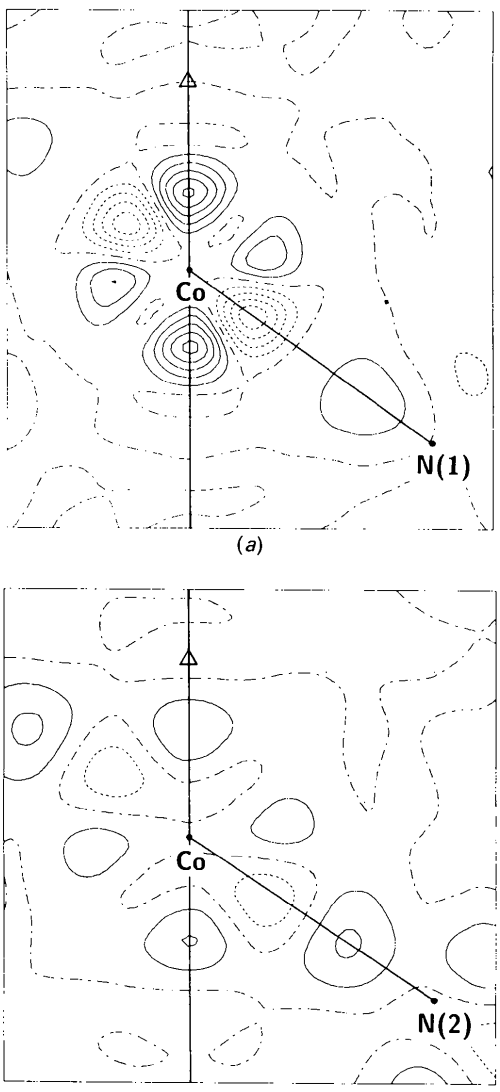

Fig. 4. Model deformation density based on only the observed reflections. (*a*) lel_3-isomer, 3916 reflections, $\sin\theta/\lambda \le 1{\cdot}08$ Å^{-1}, (*b*) ob_3-isomer, 1831 reflections, $\sin\theta/\lambda \le 0{\cdot}78$ Å^{-1}. Contour intervals at 0·2 e Å^{-3}.

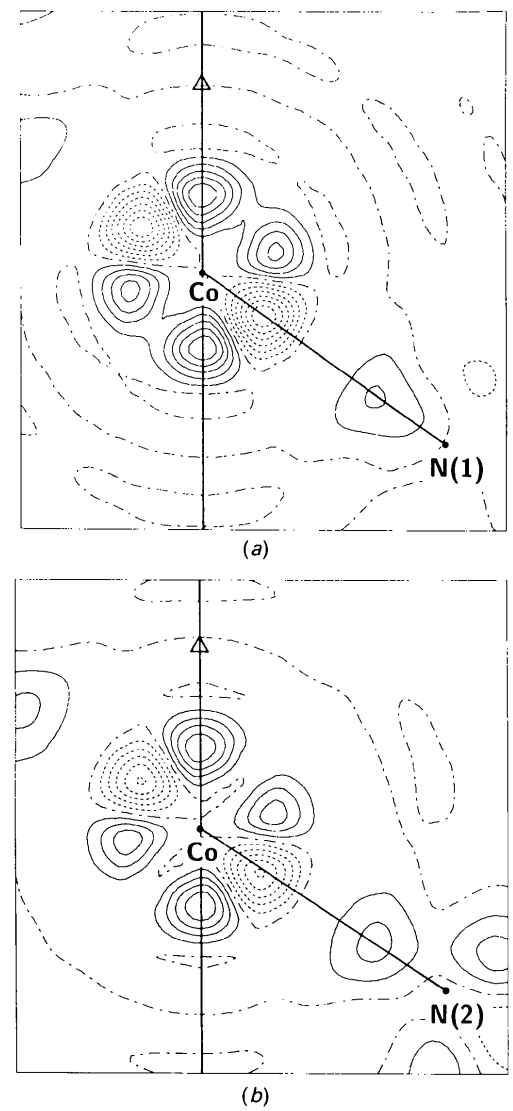

Fig. 5. Model deformation density based on all the reflections within the range of $\sin\theta/\lambda \le 1{\cdot}08$ Å^{-1}. (*a*) lel_3-isomer, 5285 reflections, (*b*) ob_3-isomer, 5350 reflections. Contour intervals at 0·2 e Å^{-3}.

in order to express the bias due to the incorrect phase angles. The c_{40} and c_{43} values of the lel_3-Co complex are 0·83 and 0·29, respectively. The deformation density ρ_{43} is much smoothed out. This is the reason why the negative trough on the Co—N bond axis is weakened before the phase improvement. Further considerations were continued to understand this peculiarity.

Multipole densities are symmetric or antisymmetric with respect to the atom center. Therefore, the Fourier transform is expressed as

$$f_{lm}(\mathbf{k}) = \tfrac{1}{2}\int \rho_{lm}(r)[\exp(2\pi i\mathbf{k}.\mathbf{r}) + s_{lm}\exp(-2\pi i\mathbf{k}.\mathbf{r})]d\mathbf{r} \quad (4)$$

where $\rho_{lm}(-\mathbf{r}) = s_{lm}\rho_{lm}(\mathbf{r})$, $s_{lm} = -1$ or 1. Since two Co atoms exist in a unit cell at $(\frac{1}{3},\frac{2}{3},0)$ and $(\frac{2}{3},\frac{1}{3},\frac{1}{2})$ related by a 2_1 screw axis along z, the structure factor for the multipole density is written as

$$F_{lm}(\mathbf{k}) = \sum_{lm} f_{lm}(\mathbf{k})\{\exp[-2\pi i(\tfrac{2h}{3}+\tfrac{k}{3})] + k_{lm}\exp[2\pi i(\tfrac{2h}{3}+\tfrac{k}{3})]\exp(l\pi i)\} \quad (5)$$

where $k_{lm} = \pm 1$, which indicates the parity of the multipole density to a rotation around z by 180°. The $F_{lm}(\mathbf{k})$ is a real or pure imaginary number depending on the parities, s_{lm} and k_{lm}, and the index l as summarized in Table 5. The contribution of Co to the structure factor in the IAM, $F_{\mathrm{IAM,Co}}$, has the identical phase to that of the monopole. The character of the $F_{40}(\mathbf{k})$ is of the same type as $F_{00}(\mathbf{k})$, because $k_{40} = s_{40} = 1$. On the other hand, the phase angle of

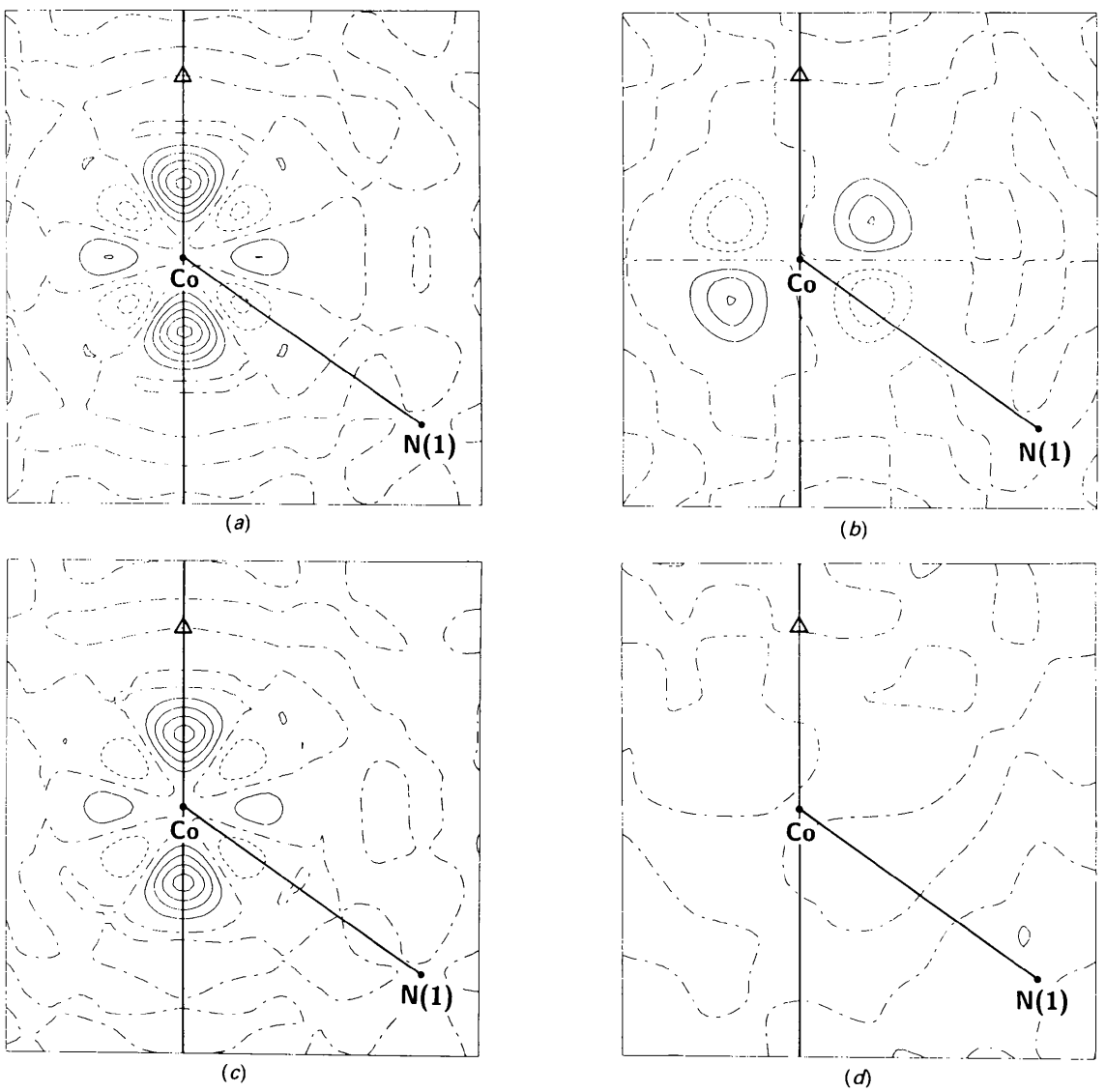

Fig. 6. Separation of the multipole densities assuming equation (2). Contour intervals at 0·2 e Å^{-3}. Phase-error free multipole densities (*a*) ρ_{40} and (*b*) ρ_{43}, and the biased densities (*c*) ρ'_{40} and (*d*) ρ'_{43}.

Table 5. *Character of the $F_{lm}(hkl)$ for the* Co *atoms in the title crystals*

(i) When $k_{lm} = 1$

	$F_{lm}(hkl)$	
s_{lm}	$l = 2n$	$l = 2n + 1$
1	Real	Pure imaginary
−1	Pure imaginary	Real

(ii) When $k_{lm} = -1$

1	Pure imaginary	Real
−1	Real	Pure imaginary

$F_{43-}(\mathbf{k})$ differs from that of $F_{00}(\mathbf{k})$ by $\pi/2$ since $k_{43-} = -1$, $s_{43-} = 1$. For reflections to which the contribution of the Co atom is large, the phase of F_{IAM} is a good approximation for F_{40}, but not for F_{43-}. An additional artificial calculation was made for the lel_3-conformer by replacing the atom scattering factors of Co with those of Rh. The damping factors of c_{40} and c_{43-} in equation (3) became 0·83→1·03 and 0·29→0·21, respectively. Therefore, the bias due to the phase error can be decreased by introducing a heavier atom center, but information on certain types of multipole densities will be still missing.

Charge asphericity

Model deformation density maps based on the observed reflection indices [(I) 3916 reflections, $\sin\theta/\lambda \le 1{\cdot}08$ Å^{-1}; (II) 1831 reflections, $\sin\theta/\lambda \le 0{\cdot}78$ Å^{-1}] are shown in Fig. 4. There are four positive peaks around the Co atom corresponding to the a_1 and e orbitals, which are of t_{2g} parentage in the O_h field. It is mysterious that the positive deformation density on the threefold axis is much higher than the other maxima although the electron population of the e orbitals, 78 (3)–80 (5)% is comparable with that of the a_1 orbital (d_{z^2}), 86 (3)–90 (5)% (see Table 4). Fig. 5 was calculated from all reflections within the range $\sin\theta/\lambda \le 1{\cdot}08$ Å^{-1} [(I) 5285, (II) 5350 reflections]. Improvement from Fig. 4(*a*) to Fig. 5(*a*) indicates that the contribution of the weak reflections [$|F_o| < 3\sigma(|F_o|)$] removed the imbalance of the positive peak heights. In addition, the features of the ob_3-isomer became clearer because of the higher resolution, $(\sin\theta/\lambda)_{max} = 1{\cdot}08$ from 0·78 Å^{-1} (Fig. 4*b* to Fig. 5*b*). Finally, typical *d*-electron distributions in the octahedral ligand field were obtained. The negative trough on the Co—N bond axis indicates the electron deficiency in the e' orbitals. The charge asphericities in the lel_3- and ob_3-conformers are similar and significant chirality was not observed, suggesting that the effect of electrostatic potential due to the C—C bond in the chelate rings is negligible for the *d* electrons to a first approximation. The nitrogen lone-pair orbital is directed along the Co—N bond axis and any offset was not detected. The Co—N(1) and Co—N(2) bond axes are inclined with respect to the threefold axis by (I) 54·55 (3) and 54·23 (4)°, and (II) 56·84 (6) and 56·27 (8)°, respectively (that for the regular octahedron is 54·74°). The small deformations of the CoN_6 chromophore from O_h symmetry, compression or elongation along the threefold axis, do not seem to be reflected in the *d*-orbital populations (see Table 4).

The model deformation density map of NO_3^- in (I) with $\sin\theta/\lambda \le 1{\cdot}08$ Å^{-1} is presented in Fig. 7. The N—O bonding and oxygen lone-pair electrons were clearly detected. Lone-pair electrons of the water oxygen atom were observed as an elongated peak on the plane bisecting the H—O—H angle. The C—C and C—N bonding electrons in the chxn ligand are also well reproduced by the multipole functions as seen from Fig. 8. Figs. 9(*a*) and 9(*b*) are the model deformation density maps on the N(1)—Co—N(2) plane of (I) calculated with the limits of $(\sin\theta/\lambda)_{max} = 1{\cdot}08$ and 1·80 Å^{-1}, respectively. The peak shape of the nitrogen lone pair is disturbed by the ripple around the Co atom, owing to a series-termination effect. Therefore, the interpretation of the small difference density in the vicinity of a high positive peak or negative trough will be meaningless. When the Co multipoles were omitted from the model deformation density, a single peak in the nitrogen

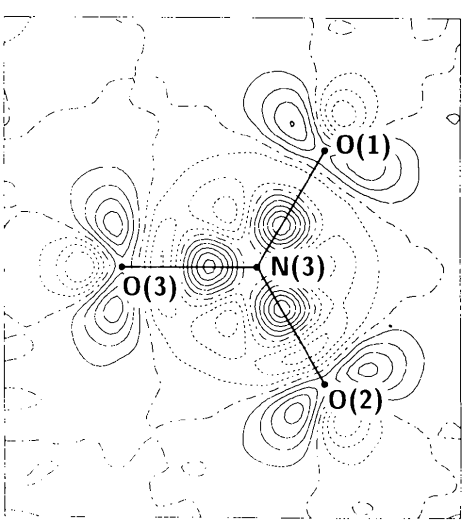

Fig. 7. Model deformation density on the NO_3 plane of the lel_3-isomer, $(\sin\theta/\lambda)_{max} = 1{\cdot}08$ Å^{-1} (5285 reflections). Contour intervals at 0·05 e Å^{-3}.

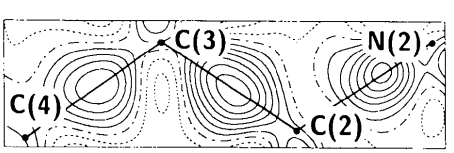

Fig. 8. Model deformation density on the plane containing the N(2)—C(2)—C(3) bond axes of the lel_3-isomer, $(\sin\theta/\lambda)_{max} = 1{\cdot}08$ Å^{-1} (5285 reflections). Contour intervals at 0·05 e Å^{-3}.

lone pair appeared even with $(\sin\theta/\lambda)_{max}$ = 1·08 Å^{-1}.

Molecular structure

The two independent Co—N bond lengths show a slight imbalance of 0·016 (1) and 0·023 (3) Å in the *lel*$_3$- and *ob*$_3$-conformers. However, there is no important difference in hydrogen bonds involving the ligating N atoms (see Table 6). The imbalance did not disappear even if the atomic coordinates were refined based on high-order reflections.

Crystals of $[M(chxn)_3](NO_3)_3.3H_2O$, M = Cr^{III}, Co^{III}, Rh^{III} and Ir^{III} are isotypes, and the M—N imbalance has been observed systematically. Therefore, the imbalance seems to be the result of crystal packing forces.

Table 6. *Hydrogen-bond distances* (Å) *involving the ligating N atoms*

(I) *lel*$_3$-isomer		(II) *ob*$_3$-isomer	
N(1)···O(2^{i})	3·114 (2)	N(1)···O(2^{iv})	2·991 (4)
N(1)···O(3^{ii})	3·125 (2)	N(2)···O(W^{v})	2·949 (5)
N(2)···O(1)	3·005 (2)	N(2)···O(3^{vi})	3·128 (6)
N(2)···O(W^{iii})	2·900 (2)	N(2)···O(W^{vi})	3·130 (4)

Symmetry code: (i) $-x+y$, $1-x$, z; (ii) $1-x$, $1-y$, $z-\frac{1}{2}$; (iii) $1-x$, $1-y$, $z+\frac{1}{2}$; (iv) $x-y$, x, $z+\frac{1}{2}$; (v) $x-y$, x, $z-\frac{1}{2}$; (vi) $1-x+y$, $1-x$, z.

We are grateful to Dr Frode Galsbøl of the H. C. Ørsted Institute, University of Copenhagen, for supplying the crystals.

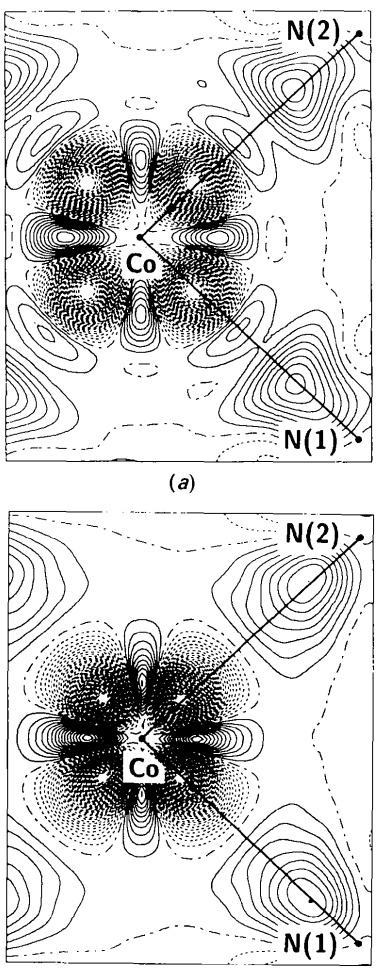

Fig. 9. Model deformation density on the N(1)—Co—N(2) plane of the *lel*$_3$-isomer. Contour intervals at 0·05 e Å^{-3}. (*a*) $(\sin\theta/\lambda)_{max}$ = 1·08 Å^{-1} (5285 reflections), (*b*) $(\sin\theta/\lambda)_{max}$ = 1·80 Å^{-1} (24255 reflections).

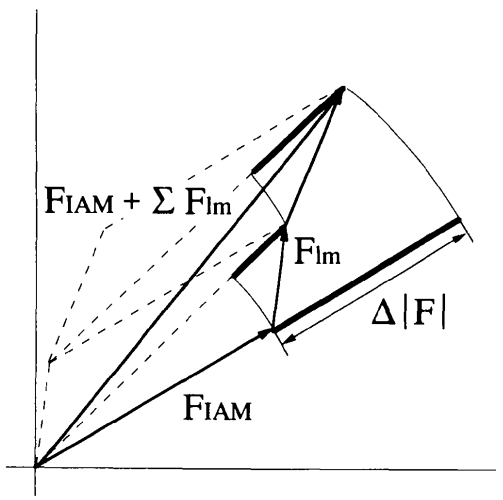

Fig. 10. Diagram of the approximation in equation (2) that $\Delta F = |F_{IAM}+\sum_{lm}F_{lm}|-|F_{IAM}| \simeq \sum_{lm}(|F_{IAM}+F_{lm}|-|F_{IAM}|)$. The value of ΔF can be estimated at summation of direct cosines of F_{lm}'s with respect to F_{IAM}. The direct cosine of F_{lm} is nearly equal to $|F_{IAM}+F_{lm}|-|F_{IAM}|$, since $|F_{lm}$'s are usually much smaller than $|F_{IAM}|$.

References

BECKER, P. J. & COPPENS, P. (1974). *Acta Cryst.* A**30**, 129–147.

BUSING, W. R. & LEVY, H. A. (1957). *Acta Cryst.* **10**, 180–182.

CLEMENTI, E. & RAIMONDI, D. L. (1963). *J. Chem. Phys.* **38**, 2686–2689.

COPPENS, P., GURU ROW, T. N., LEUNG, P., STEVENS, E. D., BECKER, P. J. & YANG, Y. W. (1979). *Acta Cryst.* A**35**, 63–72.

HAMILTON, W. C. (1959). *Acta Cryst.* **12**, 609–610.

HANSEN, N. K. & COPPENS, P. (1978). *Acta Cryst.* A**34**, 909–921.

HOLLADAY, A., LEUNG, P. & COPPENS, P. (1983). *Acta Cryst.* A**39**, 377–387.

MIYAMAE, H. (1977). Thesis. Univ. of Tokyo, Japan.

MIYAMAE, H., SATO, S. & SAITO, Y. (1977). *Acta Cryst.* B**33**, 3391–3396.

TAKAZAWA, H., OHBA, S. & SAITO, Y. (1988). *Acta Cryst.* B**44**, 580–585.